Solar-Terrestrial Physics. 2024. Vol. 10. Iss. 4. P. 72–83. DOI: 10.12737/stp-104202409. © 2024 S.I. Kozlov, S.Sh. Nikolaishvili. Published by INFRA-M Academic Publishing House

DOI: 10.12737/stp-104202409

Received June 21, 2024
Accepted August 19, 2024

SEMI-EMPIRICAL METHOD OF STUDYING THE D-LAYER AERONOMY. II. EVIDENCE-BASED CALIBRATION OF THE METHOD

S.I. Kozlov
Institute of Geosphere Dynamics RAS, Moscow, Russia, s_kozlov@inbox.ru

S.Sh. Nikolaishvili
Fedorov Institute of Applied Geophysics, Moscow, Russia, ser58ge@mail.ru

Abstract. This paper presents the results of evidence-based calibration of a new semi-empirical method for studying the D-layer aeronomy. We use simultaneous measurements of altitude profiles of electron density $N_e(h)$ and ionization rate $q(h)$ under disturbed conditions (case 1) and mean $<N_e>$ under various heliogeophysical conditions at low (LSA) and high (HSA) solar activity (case 2). The experimental data and methods are described in detail. It is shown that it is necessary to include temperature dependences of rate constants $T(h)$ for all heliogeophysical conditions. Care should be taken when choosing the $T(h)$ distribution with due regard to most of known factors having an effect on it, wherever possible. We draw a conclusion on the practicability of the use of new photodetachment rates that depend on the solar zenith angle and h. The unknown dissociative recombination rate for cluster positive ions and the photodetachment rate can be reasonably considered as free parameters, of course within due limits. Under disturbed ionospheric conditions, the evidence shows a fall in N_e at all altitudes h when $q \approx (1.3 \div 2) \cdot 10^2$ cm^{-3}s^{-1} with further increase in the parameters with q, which is confirmed by calculations using the semi-empirical model, yet for a wider range of q variations. The theoretical model that explains the aforementioned effect is the subject of future study. The results for dayside $<N_e>$ coincide qualitatively with our knowledge on the behavior of aeronomy parameters in the D layer. The studies suggest that the presented method allows qualitative estimations under all heliogeophysical conditions and even wholly satisfactory quantitative estimations under disturbed ionospheric conditions.

Keywords: lower ionosphere, missile launch, aeronomy, inverse problem.

INTRODUCTION

A semi-empirical approximate method [Kozlov et al., 2022] has been proposed to address and examine some important issues of aeronomy of the ionospheric *D*-region at different latitudes and under different heliogeophysical conditions. It allows us to identify many ionospheric features in the altitude range h~50–90 km, using the only experimental parameter — the altitude electron density profile $N_e(h)$.

In the second part of the study based on experimental data, we present the results of calibration of the method, which is a fairly simple mathematical model. For this purpose, we employ experimental data from [Whitten et al., 1965; COSPAR, 1972], derived from simultaneous measurements of $N_e(h)$ and atmospheric ionization rates $q(h)$ under conditions of artificial and natural disturbances of the *D*-region. Unfortunately, such data is very rare. This may be due to great difficulties in organizing and conducting experiments such as [Whitten et al., 1965; COSPAR, 1972; Kozlov, 2021], as well as similar ones [Kozlov, Smirnova, 1992a, b; Haerendel, Sagdeev, 1981; Avdyushin et al., 2007]. These experiments require simultaneous measurements from satellites, missiles, and with various ground-based instruments for *D*-region diagnostics. We therefore also use empirical mean $N_e(h)$ [Danilov et al., 1991; Danilov et al., 1995; Becker, 2018].

In all cases, calculations are assumed to be in satisfactory agreement with the experiment if $q(h)$ and $N_e(h)$ are simultaneously within the instrumental measurement precision. According to [Swider, Dean, 1975; Kozlov et al., 2022], such precision for the electron density depends on $N_e(h)$: at $N_e(h) \geq 10^3$ cm^{-3}, it is ±30 %; and factor 2 at $N_e(h) < 10^3$ cm^{-3}, $q(h)$ ±50 %. When calculations and experiment do not meet the above requirement, an attempt is made to improve the calculations by varying unknown or poorly understood model parameters [Kozlov et al., 2022].

1. BASIC EQUATIONS, SIMULATION TECHNIQUE, INITIAL CONDITIONS

Let us introduce the following designations: $K = \left[X_1^-\right] + \left[X_2^-\right]$ is the total concentration of primary $\left(X_1^- \equiv O_2^-\right)$ and cluster $\left[X_2^-\right]$ negative ions; $A = K + N_e = \left[X_1^+\right] + \left[X_2^+\right]$ is the condition of medium electroneutrality; $\left[X_1^+\right]$, $\left[X_2^+\right]$ are concentrations of primary and cluster positive ions. All these parameters obviously depend on h. Basic equations are

$$\begin{aligned} &\alpha_{d1}\alpha_{d2}K^3 + \left[\alpha_{d1}I_2 + \alpha_{d2}\left(2\alpha_{d1}Ne + B_{O_2^-} + I_1\right)\right]K^2 + \\ &+\left\{N_e\left[\alpha_{d1}I_2 + \alpha_{d2}\left(B_{O_2^-} + I_1 + \alpha_{d1}N_e - \beta\left[O_2\right]^2\right)\right] + \right. \\ &\left. + B_{O_2^-}I_2 + I_1I_2\right\}K - \beta\left[O_2\right]^2 N_e\left(I_2 + \alpha_{d2}N_e + B_{O_2^-}\right) = 0, \end{aligned} \quad (1)$$

$$q = \frac{\alpha_{d1}\alpha_{d2}\left(K+N_e\right)^3 + \alpha_{d2}\left(K+N_e\right)^2 B_{NO^+}}{\alpha_{d2}\left(K+N_e\right) + B_{NO^+}}, \quad (2)$$

$$\alpha_{d1}\alpha_{d2}A^3 + \alpha_{d2}B_{NO^+}A^2 - \alpha_{d2}qA - qB_{NO^+} = 0, \quad (3)$$

$$N_e = \frac{ACD}{CD + \beta\left[O_2\right]^2\left(D + B_{O_2^-}\right)}, \quad (4)$$

where α_{d1}, α_{d2} are constants of rates of dissociative recombination of $\left[X_1^+\right]$ and $\left[X_2^+\right]$ with electrons; I_1, I_2 are rates of photodetachment from $\left[X_1^-\right]$ and $\left[X_2^-\right]$ under the influence of solar radiation; β is the constant of rate of electron attachment to O_2 in triple collisions; $B_{O_2} = 6\cdot10^{-10}\left[O_3\right] + 4\cdot10^{-31}\left[O_2\right]^2$ is the rate of conversion of O_2^- to $\left[X_2^-\right]$; B_{NO+} is the effective rate of conversion of $\left[X_1^+\right]$ to $\left[X_2^+\right]$ defined by Equations (17) or (18) from [Kozlov et al., 2022]; $C=B_{O2}+I_1+\alpha_{d1}A$; $D=I_2+\alpha_{d2}A$. The above equations have been derived in [Kozlov et al., 2022] (quasi-stationary conditions). Self-consistency of Equations (1)–(4) have been confirmed by numerous calculations from the chain

$$N_{e0} \to K \to q \to A \to N_{e0} \quad (5)$$

at arbitrary N_{e0} at all altitudes under various heliogeophysical conditions.

Other known parameters characterizing the *D*-region are calculated from the following equations

$$\lambda = \frac{K}{N_e}, \quad (6)$$

$$f^+ = \frac{\left[X_2^+\right]}{\left[X_1^+\right]} = \frac{B_{NO^+}}{\alpha_{d2}A}, \quad (7)$$

$$f^- = \frac{\left[X_2^-\right]}{\left[X_1^-\right]} = \frac{2AB_{O_2^-}}{2I_2A + q}. \quad (8)$$

Effective recombination coefficient

$$\alpha_{eff} = \frac{q}{N_e^2\left(1+\lambda\right)}; \quad (9)$$

ion-ion recombination coefficient

$$\alpha_i = \frac{q}{2A^2} = \frac{\alpha_{d1} + \alpha_{d2}f^+}{2\left(1+f^+\right)}. \quad (10)$$

The calculation method for experimentally obtained N_{eexp} and q_{exp} is as follows. Substituting N_{eexp} in (1) and (2), and q_{exp} in (3) and (4), we determine model values q_m and N_{em}. Then, we check the calculations for accuracy, using the following equations

$$\Delta q = \frac{q_{exp} - q_m}{q_m}, \quad (11)$$

$$\Delta N_e = \frac{N_{eexp} - N_{em}}{N_{em}}. \quad (12)$$

The conclusion that the calculations agree with the experiment is consistent with the logic outlined in Introduction.

Using mean experimental values for $< N_{eexp} >$, proposed in [Danilov et al., 1991; Danilov et al., 1995; Friedrich, Torkar, 2001; Friedrich et al., 2018; Becker, 2018] for inclusion in deterministic (IRI type, etc. [Bekker et al., 2021; Ivanov-Kholodny, Mikhailov, 1980]) or statistical (see [Kozlov et al., 2014; Becker, 2018]) ionosphere models, yields only q_m. Unfortunately, assessment of the q_m quality is difficult and possible only when the values are compared either with general physical knowledge about the behavior of the ionization rate of the atmosphere depending on latitude, altitude, time of day, season, solar and magnetic activity, or with theoretical computations of *q*. Obviously, such assessments are purely qualitative. Nevertheless, in some cases they allow us to state some views about improving the semi-empirical method.

The initial (primary) calculation under all heliogeophysical conditions is as follows: $I_1 \approx 0.33\ s^{-1}$, $I_2 \approx 4\cdot10^{-2}\ s^{-1}$ (at night, $I_1=I_2=0$), $\alpha_{d1} = 2\cdot10^{-7}\ cm^3\ s^{-1}$, $\alpha_{d2} = 2\cdot10^{-6}\ cm^3\ s^{-1}$, $\beta = 4\cdot10^{-30}\ cm^6\ s^{-1}$ (mean value for the altitude range 50–85 km for variations in the neutral gas temperature *T* with increasing *h*); conversion rates B_{NO+} depending on $[N_2]$, $[H_2O]$, $[CO_2]$, and *T* were found from Equation (17), derived in [Kozlov et al., 2022]; whereas B_{O2-}, determined by $[O_2]$ and $[O_3]$, from the above relation; $[O_2]$, $[N_2]$, *T*, and minor neutral components of $[H_2O]$, $[CO_2]$, $[O_3]$ were estimated based on statistical processing [Bekker, 2018] of numerous experimental data from the American satellite AURA for 2004–2018. The time of day is related to the solar zenith angle χ primarily as function of latitude and *h*.

2. ANALYSIS OF EXPERIMENTAL DATA

The experiments performed at the Canadian field test site Fort Churchill (58.9° N, 265.8°E) during solar proton events (SPEs) on November 2–5, 1969 are well known [COSPAR, 1972] (see also their analysis and interpretation in [Swider, Dean, 1975; Sellers, Stroscio, 1975; Swider, 1977; Swider et al., 1978]). While simultaneous measurements of *q* and N_e [Whitten et al., 1965] were the first in geophysics, they are less known. In addition to the above work, the results were discussed in two more papers: [Swider et al., 1971] concerning estimations of α_{eff}, and [Kozlov, 1971], where an attempt was made to determine the self-consistency between measured q_{exp} and N_{eexp}, using the criterion of medium electroneutrality and a photochemical model, which was rather complex at that time. The model included four positive ions: N_2^+, O_2^+, NO^+, O^+; five negative ions: O^-, O_3^-, CO_3^-, O_2^-, NO_2^-, , and N_e. This situation might have arisen due to the fact that the measurements [Whitten et al., 1965] were made under conditions of a very specific artificial impact on the ionosphere [Kozlov, 2021] — one of the high-altitude nuclear explosions (HANE) carried out by the United States over the Pacific Ocean

at night in 1962. The authors indicated only that the ionization source was created by β products of nuclear fission, but did not give information on power, height of the explosion, distance from ground zero, and measurement time of q_{exp} and N_{eexp} after the explosion. Nevertheless, the use of data from [Whitten et al., 1965] for model calibration is in no doubt since a detailed description of the disturbance source and the conditions for obtaining experimental results is, of course, desirable, but is not a major obstacle to elaborating the model [Kozlov, 2021; Kozlov et al., 2022].

Table 1 provides a general description of missile launch conditions for the experiments described above [Swider, Dean, 1975; Whitten et al., 1965]. All launches during SPEs were performed at moderate solar activity $F10.7$=105 and high magnetic activity A_p>25. The values of $F10.7$ and A_p during the nighttime HANE are unknown. We can only note that in 1962 there was a declining phase of solar activity in the 11-year cycle. Note also that if the heights ΔH=50÷85 km are not sunlit, it is very likely that measurements of q_{exp} and N_{eexp} during HANE under the influence of β electrons of nuclear fission propagating along magnetic field lines were performed in the nearest magnetically conjugate point.

Simultaneous measurements of $N_{eexp}(h)$ [Swider, Dean, 1975; Nesterova, Ginzburg, 1985] and $q_e(h)$ [Swider, Dean, 1975], obtained during missile launches, are shown in Table 2. Note that there are few cases (~6 %) when $N_{eexp}<10^3$ cm^{-3}, and the measurement precision is low (see above). Table 1 also lists N_{eexp} and q_{exp} obtained during HANE.

From the well-known relation [Kozlov, 1971]

$$q_{exp} = (1+\lambda)^2 \alpha_{d1,d2} N_{eexp}^2, \quad (13)$$

assuming that $\alpha_i \approx \alpha_{d1}$ and $\alpha_i \approx \alpha_{d2}$ and using experimental data, we additionally calculated

Table 1

General characteristic of missile launch conditions

Conditional launch number	Date	Local time	Solar zenith angle	Time of day on the Earth surface	Measurement range measurements ΔH (km)	Time of day at altitudes ΔH
1	November 02, 1969	15:10	83°	day	44–105	day
2	November 03, 1969	06:57	96°	Dawn	64–105	day
3	November 03, 1969	07:30	92°	Dawn	60–112	day
4	November 03, 1969	12:54	75°	day	56–108	day
5	November 04, 1969	15:30	85°	day	54–103	day
6	November 04, 1969	16:38	93°	dusk	57–108	day
7	1962	no data	no data	night	50–80	night

Note. No. 1–6 — SPE, No. 7 — HANE.

Table 2

Experimental data with simultaneously measured ionization rate and electron density

Launch No., parameter \ h, km			50	55	60	65	70	75	80	85
1	N_{eexp}		$1.5\cdot10^3$	5.1·103	$1.1\cdot10^4$	$1.5\cdot10^4$	$1.7\cdot10^4$	$1.7\cdot10^4$	$2.3\cdot10^4$	$4.8\cdot10^4$
	q_{exp}		$9.0\cdot10^2$	1.0·103	$8.0\cdot10^2$	$6.3\cdot10^2$	$4.0\cdot10^2$	$3.0\cdot10^2$	$2.0\cdot10^2$	$1.3\cdot10^2$
	$\alpha_{exp}\cdot10^5$		40.54	3.86	0.65	0.29	0.13	0.10	0.04	0.01
	λ_{exp}	α_{d1}	44	13	4.7	2.8	1.6	1.3	0.35	
		α_{d2}	13	3.4	0.80	0.21				
	K_{exp}	α_{d1}	$6.6\cdot10^4$	6.6·104	$5.2\cdot10^4$	$4.1\cdot10^4$	$2.7\cdot10^4$	$2.2\cdot10^4$	$8.1\cdot10^3$	
		α_{d2}	$2.0\cdot10^4$	1.7·104	$8.9\cdot10^3$	$3.0\cdot10^3$				
	A_{exp}	α_{d1}	$6.7\cdot10^4$	7.1·104	$6.3\cdot10^4$	$5.6\cdot10^4$	$4.5\cdot10^4$	$3.9\cdot10^4$	$3.2\cdot10^4$	$4.8\cdot10^4$
		α_{d2}	$2.1\cdot10^4$	2.2·104	$2.0\cdot10^4$	$1.8\cdot10^4$	$1.7\cdot10^4$	$1.7\cdot10^4$	$2.4\cdot10^4$	$4.8\cdot10^4$
2	N_{eexp}		–	–	$1.1\cdot10^2$	$4.9\cdot10^2$	$2.5\cdot10^3$	$6.9\cdot10^3$	$1.7\cdot10^4$	$2.4\cdot10^4$
	q_{exp}		$1.3\cdot10^2$	$1.9\cdot10^2$	$1.5\cdot10^2$	$1.9\cdot10^2$	$1.9\cdot10^2$	$1.9\cdot10^2$	$1.9\cdot10^2$	$1.9\cdot10^2$
	$\alpha_{exp}\cdot10^5$		–	–	–	80.77	3.02	0.39	0.07	0.03
	λ_{exp}	α_{d1}	–	–	–	63	11	3.4	0.86	0.27
		α_{d2}	–	–	–	19	2.9	0.39		
	K_{exp}	α_{d1}	–	–	–	$3.0\cdot10^4$	$2.8\cdot10^4$	$2.4\cdot10^4$	$1.4\cdot10^4$	$6.6\cdot10^3$
		α_{d2}	–	–	–	$9.3\cdot10^3$	$7.2\cdot10^3$	$2.8\cdot10^3$		

Launch No., parameter \ h, km			50	55	60	65	70	75	80	85
	A_{exp}	α_{d1}	–	–	–	$3.1\cdot10^4$	$3.1\cdot10^4$	$3.1\cdot10^4$	$3.1\cdot10^4$	$3.1\cdot10^4$
		α_{d2}	–	–	–	$9.7\cdot10^3$	$9.7\cdot10^3$	$9.7\cdot10^3$	$1.7\cdot10^4$	$2.4\cdot10^4$
3	N_{eexp}		–	–	$1.7\cdot10^2$	$1.9\cdot10^3$	$5.0\cdot10^3$	$8.7\cdot10^3$	$1.5\cdot10^4$	$2.6\cdot10^4$
	q_{exp}		$1.3\cdot10^2$	$1.9\cdot10^2$	$1.5\cdot10^2$	$1.9\cdot10^2$	$1.9\cdot10^2$	$1.9\cdot10^2$	$1.9\cdot10^2$	$1.9\cdot10^2$
	$\alpha_{exp}\cdot10^5$		–	–	507.03	5.05	0.75	0.25	0.08	0.03
	λ_{exp}	α_{d1}	–	–	$1.6\cdot10^2$	15	5.1	2.6	1.1	0.17
		α_{d2}	–	–	49	4	0.94	0.13		
	K_{exp}	α_{d1}	–	–	$2.7\cdot10^4$	$2.9\cdot10^4$	$2.6\cdot10^4$	$2.2\cdot10^4$	$1.6\cdot10^4$	$4.4\cdot10^3$
		α_{d2}	–	–	$8.5\cdot10^3$	$7.8\cdot10^3$	$4.7\cdot10^3$	$1.1\cdot10^3$		
	A_{exp}	α_{d1}	–	–	$2.7\cdot10^4$	$3.1\cdot10^4$	$3.1\cdot10^4$	$3.1\cdot10^4$	$3.1\cdot10^4$	$3.1\cdot10^4$
		α_{d2}	–	–	$8.7\cdot10^3$	$9.7\cdot10^3$	$9.7\cdot10^3$	$9.7\cdot10^3$	$1.5\cdot10^4$	$2.6\cdot10^4$
4	N_{eexp}		–	$1.7\cdot10^3$	$3.3\cdot10^3$	$4.6\cdot10^3$	$7.2\cdot10^3$	$1.5\cdot10^4$	$3.4\cdot10^4$	$4.7\cdot10^4$
	q_{exp}		$8.0\cdot10^1$	$1.0\cdot10^2$	$9.0\cdot10^1$	$1.0\cdot10^2$	$1.2\cdot10^2$	$1.2\cdot10^2$	$1.2\cdot10^2$	$1.3\cdot10^2$
	$\alpha_{exp}\cdot10^5$		–	3.27	0.81	0.47	0.23	0.05	0.01	0.01
	λ_{exp}	α_{d1}	–	12	5.4	3.9	2.4	0.60		
		α_{d2}	–	3.0	1.0	0.54	0.08			
	K_{exp}	α_{d1}	–	$2.1\cdot10^4$	$1.8\cdot10^4$	$1.8\cdot10^4$	$1.7\cdot10^4$	$9.2\cdot10^3$		
		α_{d2}	–	$5.3\cdot10^3$	$3.4\cdot10^3$	$2.5\cdot10^3$	$5.6\cdot10^2$			
	A_{exp}	α_{d1}	–	$2.2\cdot10^4$	$2.1\cdot10^4$	$2.2\cdot10^4$	$2.4\cdot10^4$	$2.4\cdot10^4$	$3.4\cdot10^4$	$4.7\cdot10^4$
		α_{d2}	–	$7.1\cdot10^3$	$6.7\cdot10^3$	$7.1\cdot10^3$	$7.7\cdot10^3$	$1.5\cdot10^4$	$3.4\cdot10^4$	$4.7\cdot10^4$
5	N_{eexp}		$1.5\cdot10^2$	$4.8\cdot10^2$	$1.4\cdot10^3$	$2.7\cdot10^3$	$3.6\cdot10^3$	$4.8\cdot10^3$	$8.3\cdot10^3$	$1.1\cdot10^4$
	q_{exp}		$1.0\cdot10^1$	$1.5\cdot10^1$	$2.0\cdot10^1$	$2.2\cdot10^1$	$2.5\cdot10^1$	$2.5\cdot10^1$	$2.5\cdot10^1$	$2.5\cdot10^1$
	$\alpha_{exp}\cdot10^5$		–	6.51	1.01	0.30	0.19	0.11	0.04	0.02
	λ_{exp}	α_{d1}	–	17	6.1	2.9	2.1	1.3	0.33	0.02
		α_{d2}	–	4.7	1.2	0.23				
	K_{exp}	α_{d1}	–	$8.2\cdot10^3$	$8.6\cdot10^3$	$7.8\cdot10^3$	$7.6\cdot10^3$	$6.4\cdot10^3$	$2.8\cdot10^3$	$1.8\cdot10^2$
		α_{d2}	–	$2.3\cdot10^3$	$1.8\cdot10^3$	$6.2\cdot10^2$				
	A_{exp}	α_{d1}	–	$8.7\cdot10^3$	$1.0\cdot10^4$	$1.0\cdot10^4$	$1.1\cdot10^4$	$1.1\cdot10^4$	$1.1\cdot10^4$	$1.1\cdot10^4$
		α_{d2}	–	$2.7\cdot10^3$	$3.2\cdot10^3$	$3.3\cdot10^3$	$3.6\cdot10^3$	$4.8\cdot10^3$	$8.4\cdot10^3$	$1.1\cdot10^4$
6	N_{eexp}		–	$3.6\cdot10^2$	$6.8\cdot10^2$	$2.0\cdot10^3$	$3.9\cdot10^3$	$4.4\cdot10^3$	$7.4\cdot10^3$	$1.2\cdot10^4$
	q_{exp}		$1.0\cdot10^1$	$1.4\cdot10^1$	$1.9\cdot10^1$	$2.0\cdot10^1$	$2.3\cdot10^1$	$2.3\cdot10^1$	$2.3\cdot10^1$	$2.3\cdot10^1$
	$\alpha_{exp}\cdot10^5$		–	–	4.21	0.48	0.15	0.12	0.04	0.02
	λ_{exp}	α_{d1}	–	–	14	3.9	1.7	1.5	0.45	
		α_{d2}	–	–	3.6	0.54				
	K_{exp}	α_{d1}	–	–	$9.1\cdot10^3$	$8.0\cdot10^3$	$6.8\cdot10^3$	$6.4\cdot10^3$	$3.3\cdot10^3$	
		α_{d2}	–	–	$2.4\cdot10^3$	$1.1\cdot10^3$				
	A_{exp}	α_{d1}	–	–	$9.7\cdot10^3$	$1.0\cdot10^4$	$1.1\cdot10^4$	$1.1\cdot10^4$	$1.1\cdot10^4$	$1.2\cdot10^4$
		α_{d2}	–	–	$3.1\cdot10^3$	$3.2\cdot10^3$	$3.9\cdot10^3$	$4.4\cdot10^3$	$7.4\cdot10^3$	$1.2\cdot10^4$
7	N_{eexp}		$1.3\cdot10^3$	$3.4\cdot10^4$	$5.0\cdot10^4$	$8.0\cdot10^4$	$2.4\cdot10^5$	$2.7\cdot10^5$	$1.4\cdot10^5$	–
	q_{exp}		$7.0\cdot10^4$	$1.3\cdot10^5$	$1.36\cdot10^5$	$1.15\cdot10^5$	$9.2\cdot10^4$	$7.0\cdot10^4$	$4.0\cdot10^4$	–
	$\alpha_{exp}\cdot10^5$		4142.01	11.25	5.44	1.80	0.16	0.09	0.21	–
	λ_{exp}	α_{d1}	$4.5\cdot10^2$	23	15	8.5	1.8	1.2	2.3	–
		α_{d2}	$1.4\cdot10^2$	6.5	4.2	2.0			0.03	–
	K_{exp}	α_{d1}	$5.9\cdot10^5$	$7.7\cdot10^5$	$7.7\cdot10^5$	$6.8\cdot10^5$	$4.4\cdot10^5$	$3.2\cdot10^5$	$3.1\cdot10^5$	–
		α_{d2}	$1.9\cdot10^5$	$2.2\cdot10^5$	$2.1\cdot10^5$	$1.6\cdot10^5$			$4.4\cdot10^3$	–
	A_{exp}	α_{d1}	$5.9\cdot10^5$	$8.1\cdot10^5$	$8.2\cdot10^5$	$7.6\cdot10^5$	$6.8\cdot10^5$	$5.9\cdot10^5$	$4.5\cdot10^5$	–
		α_{d2}	$1.9\cdot10^5$	$2.5\cdot10^5$	$2.6\cdot10^5$	$2.4\cdot10^5$	$2.4\cdot10^5$	$2.7\cdot10^5$	$1.4\cdot10^5$	–

Table 3

Altitudes h' at which $\lambda=1$ for different α_{d1} and α_{d2}

Launch number	1	2	3	4	5	6	7
h' (α_{d1})	76.6	79.9	80.5	73.9	76.5	77.4	–
h' (α_{d2})	59.6	73.8	69.9	60.0	61.0	64.2	72.6

$$\alpha_{exp} = \frac{q_{exp}}{N_{eexp}^2}, \quad (14)$$

$$\lambda_{exp} = \frac{1}{N_{eexp}}\left(\frac{q_{exp}}{\alpha_{d1,d2}}\right)^{1/2} - 1, \quad (15)$$

$$K_{exp} = \left(\frac{q_{exp}}{\alpha_{d1,d2}}\right)^{1/2} - N_{eexp}, \quad (16)$$

$$A_{exp} = K_{exp} + N_{eexp} = \left(\frac{q_{exp}}{\alpha_{d1,d2}}\right)^{1/2} = \left[X_1^+\right] + \left[X_2^+\right]. \quad (17)$$

From (15), (16) we can easily derive a relation for the critical value of the dissociative recombination rate constant

$$\alpha_{d1,\,d2} < \alpha_{exp}, \quad (18)$$

when λ_{exp} and K_{exp} remain positive, i.e. they have a physical meaning. The results of calculation from (14)–(17) are given in Table 2 for $\alpha_{d1}=2\cdot10^{-7}$cm^3 s^{-1} and $\alpha_{d2}=2\cdot10^{-6}$cm^3 s^{-1}. Empty cells in lines λ_{exp}, K_{exp} indicate the case when condition (18) is not met; squares "–", the absence of experimental data.

It is advisable to conduct an in-depth analysis of the data in Table 2, which will allow us to determine the most optimal ways to improve the semi-empirical model in the future.

Values of λ_{exp}, K_{exp}, and A_{exp} are cross-linked and depend on α_{d1} and α_{d2}. With an increase in h, λ_{exp}, K_{exp} should decrease, and the medium electroneutrality condition A_{exp} should remain approximately constant [Kozlov, 2021], which is in fact observed in Table 2.

Table 3 lists h' where $\lambda_{exp}=1$. Obviously, at α_{d2}, h' decreases. For all launches, the use of α_{d2} causes the violation of condition (18) at high altitudes. This situation takes place at α_{d1} only in two cases — at $h\geq80$ km for launch No. 4 and at h=85 km for launch No. 6. All these suggest that it is likely impossible to consider α_{d1} and α_{d2} constant in the h range of interest. In launch No. 7 (HANE, night) even at α_{d1}, λ_{exp} does not exceed 1; and at α_{d2} at altitudes of 70 and 75 km, $\lambda_{exp}<0$. Linear approximation between adjacent points allowed us to approximately find λ_{exp}(70 km)=1.34, λ_{exp}(75 km)=0.69. To find h' from (15) requires $\alpha_{d1}=\alpha_e$, which is unrealistic.

The need to use the profiles $\alpha_{d1}(h)$ and $\alpha_{d2}(h)$ is confirmed by $A_{exp}(h)$ in all launches. In the lower part of the D-region, where the role of negative ions is great, for both coefficients $A_{exp}=K_{exp}>N_{eexp}$, $\lambda_{exp}>1$ (it is especially clear at h=50 km, where, unfortunately, simultaneous measurements of q and N_e were performed only in two cases). At high altitudes, $A_{exp}=N_{eexp}$, $\lambda_{exp}<1$. The best agreement between A_{exp} and N_{eexp} at $\alpha_{d2}=2\cdot10^{-6}$cm^3 s^{-1} was unexpected, which by definition refers either to cluster ions X_2^+, or to the unknown ion-ion recombination coefficient α_i. In this case, $\alpha_{d2}\neq\alpha_{exp}$ at the altitudes, where the equality $A_{exp}=N_{eexp}$ holds. The reasons for this situation are discussed in the next section.

Of particular interest is the analysis of variations in $N_{eexp}(q_{exp}, h)$, which are illustrated in Figure 1. It allows us to evaluate the self-consistency of measured N_{eexp} and q_{exp}, using simple physical arguments for the electron density in the disturbed D-region [Kozlov, 1971; Smirnova et al., 1990]: at any altitude, N_e increases with ionization rate. Of course, Figure 1 is approximate due to the lack of experimental data and linear approximation. Nevertheless, the above tendency is evident at all h. The exception is $q_{exp}\approx(1.3\div2)10^2$ cm^{-3} s^{-1}, where at $h>55$ km N_e decreases in launches 1–3 even when points with $N_{eexp}<10^3$ cm^{-3} are excluded. This may be due to the precision in measurements of N_{eexp} and q_{exp}. This effect is detailed in Section 3.

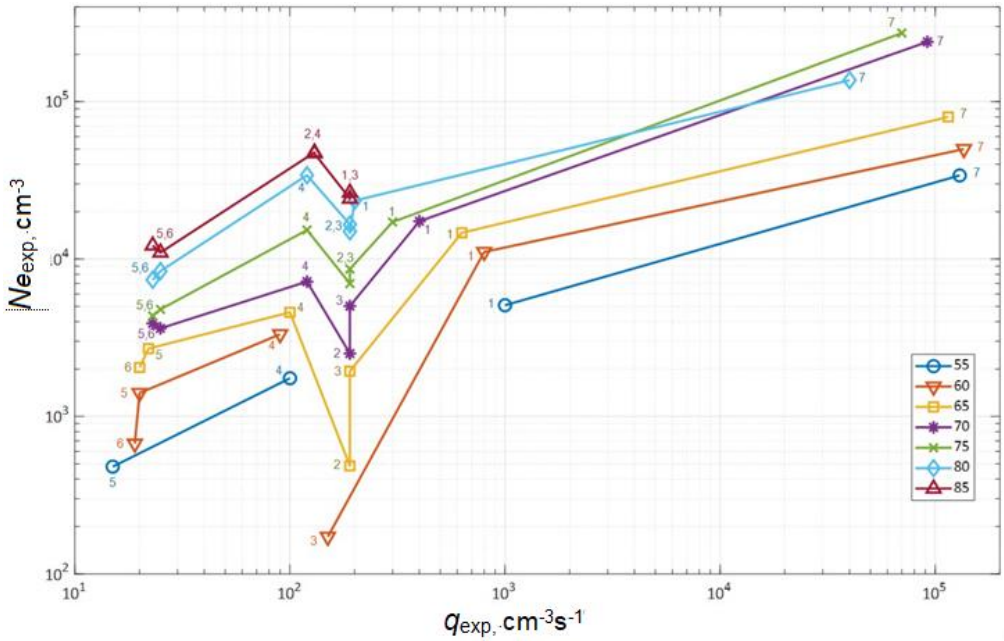

Figure 1. N_{eexp} as function of q_{exp} at different altitudes. The numbers near symbols indicate the launch number (see Table 1)

To calibrate the model with empirical mean $<N_{eexp}>$, we have used only data from [Becker, 2018], which was obtained from fairly complete statistical processing of the catalog [Nesterova, Ginzburg, 1985] and was more representative than in [Danilov et al., 1991; Danilov et al., 1995]. The data is presented in Figure 2 for low (LSA, left) and high (HSA) solar activity. In this case, the quality of model calculations was assessed from q, λ, and α_{eff}, using a logic chain (Figure 3) based on well-known ideas on the behavior of these values in the D-region.

3. CALCULATION RESULTS AND THEIR DISCUSSION

Since the model is calibrated using two experimental data sets, obtained under disturbed (N_{eexp}, q_{exp}) and quiet ($<N_{eexp}>$) conditions, it is worth first discussing the results of calculations from the data separately, and then try to draw general conclusions.

3.1. Figures 4, 5 present the results of calculations of Δq and ΔN_e from Equations (11) and (12) in terms of the initial data set from Section 1.

From Table 2 it is easy to find that the total number of measurements of N_{eexp} and q_{exp} for all missile launches with an altitude step h=5 km is $S(N_{eexp}, q_{exp})$=104 of which $S(N_e)$=49, $S(q_{exp})$=55.

Figures 4, 5 show that the number of calculations, in which both N_{em} and q_m were simultaneously within the instrumental precision, was only 1 case or $1\cdot100/S(N_{eexp}, q_{exp})\approx1$ (as a percentage); the number of estimates of N_{em} within the precision turned out to be 5 or $5\cdot100/S(N_{eexp})\approx10.2$; calculations of q_m, 3 or $3\cdot100/S(q_e)\approx6.7$ of $S(q_e)$=49 since the absence of N_{eexp} in some cases did not allow us to find q_m.

The presented estimates for comparing model calculations with experimental data are conventionally called point estimates.

Another approach is based on the well-known principles of geometric probability. The calculations were carried out with an altitude step h=5 km (see Table 2), and linear interpolation between the points (see Figures 4, 5). It is evident that there are cases when two adjacent points are beyond the range of the instrumental precision of q, N_e measurements, and part of the straight line l connecting them passes through this range. This is valid for all other cases: a part of the unified curves of Δq and ΔN_e coincides with the range of instrumental precision; the other does not. Then, the quality of calculations is determined by the probability $P(q, N_e)=l/L$, where L is the total curve length. It is clear that $0<P(q, N_e)<1$.

As expected, this method allowed us to improve the results: $P(q, N_e)\approx0.10$ (when both q and N_e are simultaneously within the instrumental precision), $P(N_e)\approx0.12$, $P(q)\approx0.19$.

The question arises whether the above point and geometric estimates are valid or not, given that they are initial and no attempts have been made to improve the method. The answer depends on requirements for the precision imposed on a particular problem: in some cases, the calculation results can be considered satisfactory; in others cannot.

The first step to improve the semi-empirical method is to reject the mean (constant) values of β, α_{d1}, α_{d2}, which agrees with the conclusion from the analysis of experimental data in Table 2.

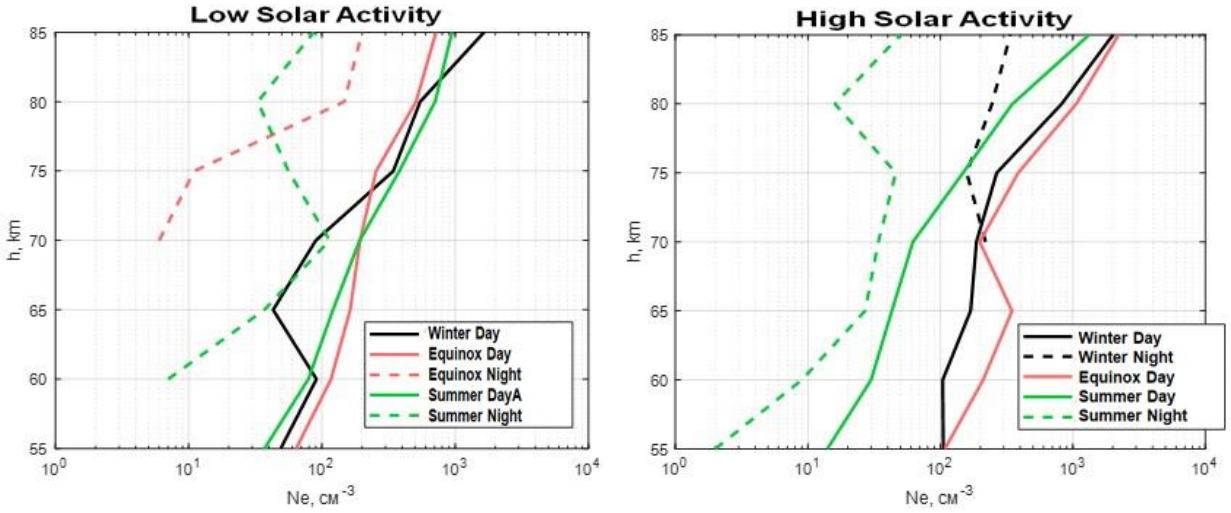

Figure 2. Vertical profiles of N_e for different heliogeophysical conditions from the catalog [Nesterova, Ginzburg, 1985]

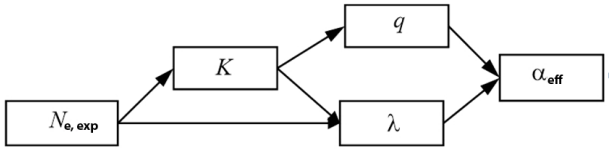

Figure 3. Logic chain for determining q, λ, and α_{eff}

Equations (1)–(4) are complemented by the expressions

$$\beta = 1.4\cdot10^{-29}\left(300/T\right)\exp\left(600/T\right), \quad (20)$$

$$\alpha_{d1} = 4\cdot10^{-7}\left(300/T\right)^{1.5}, \quad (21)$$

$$\alpha_{d2} = 2\cdot10^{-6}\left(300/T\right)^{0.5}, \quad (22)$$

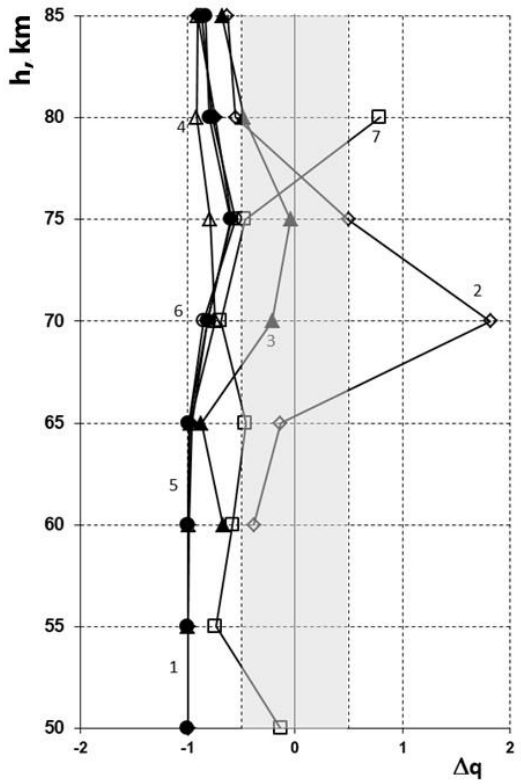

Figure 4. Calculation of Δq_n for launches 1–6 (day, I_1=0.33 s^{-1}, I_2=0.04 s^{-1}), 7 (night, I_1=I_2=0), α_{d1}=2·10^{-7}cm^3 s^{-1}, α_{d2}=2·10^{-6} cm^3 s^{-1}, β=4·10^{-30} cm^6 s^{-1}. The gray field indicates the q measurement precision

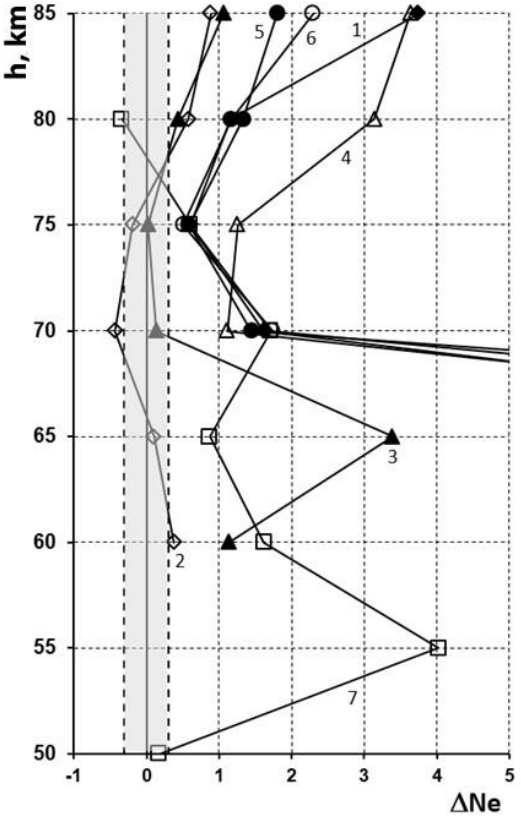

Figure 5. ΔN_e for launches 1–6 (day, I_1=0.33 s^{-1}, I_2=0.04 s^{-1}), 7 (night, I_1=I_2=0), α_{d1}=2·10^{-7}cm^3 s^{-1}, α_{d2}=2·10^{-6} cm^3 s^{-1}, β=4·10^{-30} cm^6 s^{-1}. The gray field is the N_e measurement precision

the first two of which are quite well known due to laboratory experiments and have been taken according to [Kozlov et al., 2022], and the last one is hypothesized due to the lack of reliable theoretical calculations and experimental data (see, e.g., [Boyarchuk et al., 2006; Gordillo Vazquez, 2008; Van Gaens, Bogaerts, 2013]). Thus, α_{d2} should be considered as a freely variable parameter. Note also that substitution of $T(h)$, which actually exist in the ionosphere, in (20)–(22) leads to complex variations in N_e because β decreases, α_{d1} and α_{d2} increase. Using $T(h)$ from Aura satellite data yields $S(q, N_e)$≈10.2 %, $P(q, N_e)$≈0.14; $S(N_e)$=14.3 %, $P(N_e)$=0.17; $S(q)$≈16.3 %, $P(q)$≈0.25. These estimates are seen to be much better than the previous ones. Since temperatures at 50–85 km are relatively unstable and depend on many factors (temperature at h<50 km, latitude, season, etc.), calculations were performed with the distribution $T(h)$, taken from the well-known global neutral atmosphere model MSIS-90. The fundamental difference between MSIS and Aura data is that $T(h)$ is larger at some h. We have obtained the following results: $S(q, N_e)$≈10.2 %, $P(q, N_e)$≈0.16; $S(N_e)$≈10.2 %, $P(N_e)$≈0.20; $S(q)$≈18.4 %, $P(q)$≈0.27. Note that the most significant improvement is observed for $S(q)$ and $P(q)$. This is important for estimating q from experimental measurements of N_{eexp} (see Item 3.2).

It turned out to be very interesting to employ a new coefficient of photodetachement from $X_1^- \equiv O_2^-$, obtained in [Kozlov, Lyakhov, 2023], taking into account h, χ, solar activity, new cross-sections of photodetachement from O_2^-, recent solar emission spectra in the range λ=120–800 nm, and more adequate models of the atmosphere (unlike [World Meteorological Organization, 1985]) through which this emission passes. When using the $T(h)$ distribution from MSIS-90 for daytime missile launches 1–6, $S(q, N_e)$=19.0 %, $P(q, N_e)$=0.16; $S(N_e)$=21.4 %, $P(N_e)$=0.2; $S(q)$=26.2 %, $P(q)$=0.27. These are the best estimates as compared to those obtained earlier.

The agreement of calculations with the experiment can further be improved by varying the little-known parameters α_{d2} and I_2. The need to correctly determine α_{d2} and I_2 is very clearly and convincingly demonstrated in Figure 6 by comparing the median mean experimental values of $\alpha_{exp}(h)$, derived from Table 2, with model calculations. $\alpha_m(h) = q_m(h)/N_{em}^2(h)$.

First, we calculated median $<\alpha_m(h)>$, taking into account T dependent rates, new values for I_1, and $T(h)$ from MSIS-90 (curve 1). It is clear that $\alpha_m > \alpha_{exp}$ at almost all altitudes and especially at h<70 km. To bring the experiment and calculations closer together, we must either decrease q_m or increase N_{em}, or both. This can be achieved by decreasing α_{d2}, derived from Equation (22), or by increasing I_2 from the initial value 0.04 s^{-1} (see Section 1). Some calculation results with varying α_{d2} and I_2 are presented in Figure 6. Obviously, the parameters α_{d2} and I_2 cannot be considered constant at h of interest. Moreover, in the upper part of the D-region, the dissociative recombination of

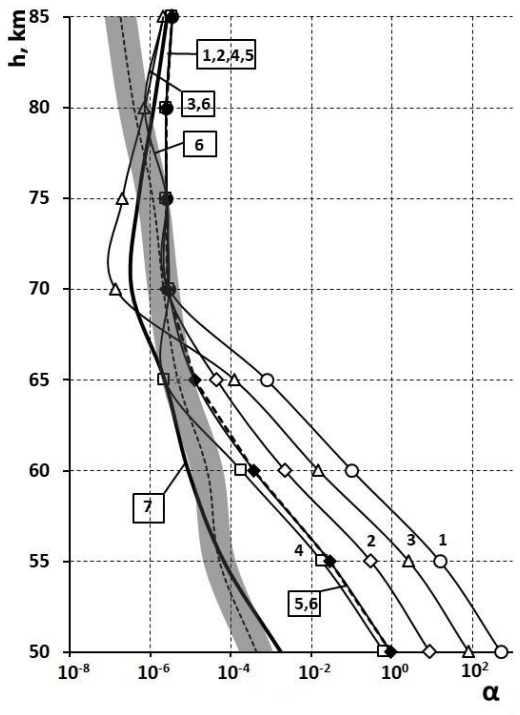

Figure 6. Comparison of experimental values $<\alpha_{exp}>$ with model calculations $<\alpha_m>$ when varying unknown parameters α_{d2} and I_2. The gray field is the precision of measurements of α_{exp} and its median. Calculation results: 1 — taking into account T dependent rates, new values of I_1 [Kozlov, Lyakhov, 2023], I_2=0.04 s^{-1}, $T(h)$ from MSIS-90; 2 — the same, but I_2=0.2 s^{-1}; 3 — the same, $0.2\alpha_{d2}(T)$, I_2=0.04 s^{-1}; 4 — I_2=0.2 s^{-1}, $0.2\alpha_{d2}(T)$ at $h\leq65$ km; 5 — I_2=0.4 s^{-1}; 6 — I_2=0.4 s^{-1} at $h\leq65$ km, $0.2\alpha_{d2}(T)$ at $h\geq80$ km; 7 — $0.2\alpha_{d2}$ at $h\leq65$ km, $0.33\alpha_{d2}$ at $h>65$ km; I_2=1 s^{-1} at $h<60$ km, I_2=0.5 s^{-1} at h=60 km, I_2=0.2 s^{-1} at h=60 km, I_2=0.8 s^{-1} at $h>65$ km

positive ions with electrons dominates, although the influence of negative ions is noticeable; in the lower part, the photodetachement of electrons from cluster ones X_2^-. Figure 6 suggests that it is reasonable to simultaneously change both parameters according to h. The best agreement with the experiment is obtained if at $h\leq75$ km we assume I_2=0.2 s^{-1}, $0.2\alpha_{d2}$; at $h>75$ km, I_2=0.04 s^{-1}, $0.2\alpha_{d2}$ (curves 3, 4, 6). Yet, the question remains unanswered at $h<60$ km, where $\alpha_m(h)>\alpha_{exp}(h)$. It is presumably necessary to use the value $I_2>0.4$ s^{-1}, implying that it includes not only the photodetachment of electrons from X_2^-, but also detachment from them in collisions with neutral components in ground and excited states. This consideration is supported by calculations (Figure 6, curve 7). The agreement with the experiment can be considered almost perfect. Especially noteworthy is that $I_2(h)$ and $\alpha_{d2}(h)$ are consistent with the general physical concepts: the decrease in I_2 with increasing h is well explained by a decrease in atmospheric density, which automatically reduces the contribution of electron detachment from X_2^- in collisions, and, in addition, by changes in the composition of negative ions during SPEs; different values of α_{d2} are primarily defined by the hypothetical nature of Equation (22), which at real ionospheric T yields $\alpha_{d2}>2\cdot10^{-6}$ cm^3 s^{-1} (see Section 1).

Figures 7, 8 present the results of calculations of Δq and ΔN_{eexp} made at $I_2(h)$ and $\alpha_{d2}(h)$, used for estimating $<\alpha_m>$ (see Figure 6, curve 7).

Analysis of the estimates allows us to draw two important conclusions: 1) reasonable selection of $\alpha_{d2}(h)$ and $I_2(h)$ allows us to obtain quite satisfactory theoretical results; in our case, $S(q, N_e)$=31 %, $P(q, N_e)$=0.33; $S(q)$=47.6 %, $P(q)$=0.42; $S(N_e)$=40.5 %, $P(N_e)$=0.52; 2) The described approach is advisable to apply to model calculations when analyzing experimental data acquired in each missile launch, which will enable us to evaluate the dependences of α_{d2} and I_2 not only on altitude, but also on time of day, since the launches were conducted at different times (see Table 1).

The results of the step-by-step calibration of the method are summarized in Table 4. At each subsequent step, the positive results obtained at previous steps are taken into account.

In conclusion, it is worth noting that for N_{eexp} and q_{exp} from other SPEs or solar X-ray flares of various classes the quantitative estimates can change.

3.2. Using $<N_e>$ to calibrate the semi-empirical method allows us to draw only qualitative conclusions about the model as a whole. On the other hand, unlike Item 3.1., they make it possible to test the method in a wide range of heliogeophysical conditions (in this case, for 10 (see Figure 2)). The calculations have been carried out using the logic chain (see Figure 3) from Equations (20)–(22) and the model of neutral components, determined from Aura satellite data for midlatitudes.

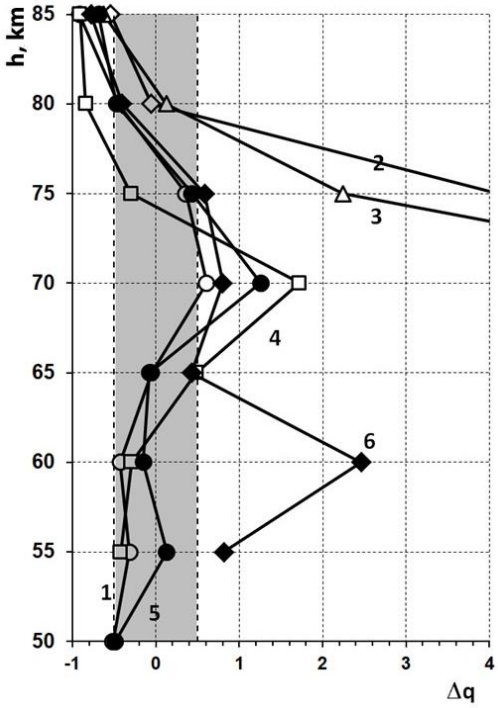

Figure 7. Calculation of Δq for launches 1–6 with regard to T dependent rates, new values I_1, $T(h)$ from MSIS-90; $\alpha_{d2}(h)$ and $I_2(h)$ correspond to the values used in calculations of curve 7 in Figure 6

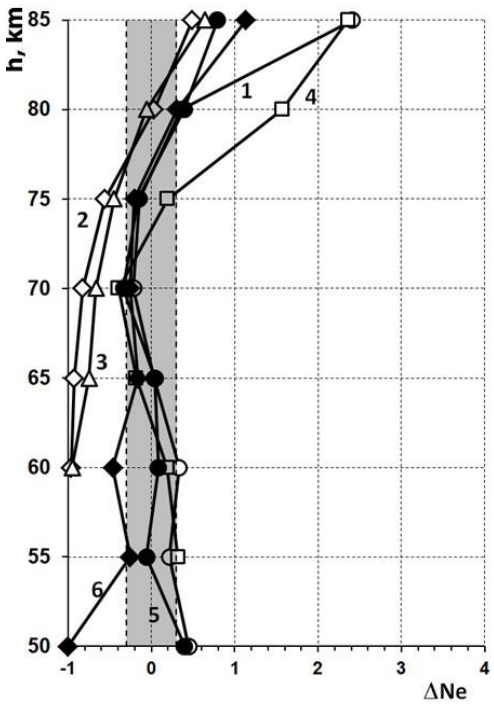

Figure 8. Calculation of ΔN_e for launches 1–6, taking into account T dependent rates, new values I_1, $T(h)$ from the MSIS-90; $\alpha_{d2}(h)$ and $I_2(h)$ are the values used in calculations of curve 7 in Figure 6

The altitude profiles of K, λ, α_{eff} are beyond any doubt for all ten heliogeophysical conditions: they decrease with increasing h. At the same time, the nighttime values, as expected, are higher than the daytime ones.

It is interesting to change the calculated q from h for given $<N_e>$ (Figure 9, *a*, *b*). During the day, $q(h)$ can be roughly divided into three ranges:

1) h>75 km. The main source is the ionization of N_2, O_2, and partly O by solar radiation. Increasing I_1 has a very weak effect on q; season and solar activity are much more important.

2) 75 km ≥h≥66–67 km. Here, NO and $O_2(^1\Delta_g)$ are ionized by solar radiation in the Lα and Lβ lines. In this case, negative ions (via I_1) begin to significantly affect q, reducing it.

3) h < 66–67 km. It is obvious that the ionization of the medium is caused by cosmic rays, which increases in direct proportion to decreasing h. Unfortunately, it is not always possible to increase q when solar activity decreases, which is likely due to large inaccuracies in the N_e measurements, included in the database [Nesterova, Ginzburg, 1985], in the lower part of the D-region. A change in I_1 is seen to affect q, but to a lesser extent compared to the previous range since at h <66–67 km $\left[X_2^-\right] >> \left[X_1^-\right]$, λ>1 under all heliogeophysical conditions.

At night, the volume of catalog data [Nesterova, Ginzburg, 1985] is significantly smaller than that of daytime data. That is why, in Figure 9, *b* we present only four cases of calculations. The altitudes, at which there are minimum q, increase due to increasing solar zenith angles. At h<75 km, it can be seen that mainly in summer q(LSA)>q(HSA). We, however, have no explanation for the flat profile of q at h<65–70 km; either this is due to errors in experimental measurements, as mentioned above, or incomplete knowledge about processes in the D-region. In general, the problem of nighttime D-layer ionization below ~90–100 km remains unresolved. This consideration is supported by the inexplicable oscillation of $q(h)$ under equinox conditions.

Analysis of the behavior of q depending on $<N_e>$ did not lead to any other conclusions differing from those formulated above when discussing the results in Figure 9.

Thus, the semi-empirical method [Kozlov et al., 2022] is valid under various heliogeophysical conditions and requires only experimental data on $N_e(h)$. Note that in some cases the estimates will be only qualitative (the standard deviations of $<N_e>$ used here are very large [Bekker, 2018]).

Table 4

Overall results of step-by-step calibration of the model for known N_{eexp} and q_{exp}

Stage number	Parameters	Results (points), %		Results (geometry)	
		ΔN_e	Δq	ΔN_e	Δq
0	Initial calculation: coefficients I_1, I_2, β, α_{d1}, α_{d2} do not vary with height h; neutral composition is from Aura satellite data	10.2	6.7	0.12	0.19
		1.0		0.10	
1	Calculation of β, α_{d1}, α_{d2} from Equations (20)–(22); temperature $T(h)$ from Aura satellite data	14.3	16.3	0.17	0.25
		10.2		0.14	
2	Calculation of β, α_{d1}, α_{d2} from Equations (20)–(22); temperature $T(h)$ from MSIS-90	10.2	18.4	0.20	0.27
		10.2		0.16	
3	Calculation of β, α_{d1}, α_{d2} from Equations (20)–(22); temperature $T(h)$ from MSIS-90; photodetachment coefficient I_1 from [Kozlov, Lyakhov, 2023]. Analysis for 6 daytime launches	21.4	26.2	0.20	0.27
		19.0		0.16	
4	Calibration of the model by α=q/N_e^2. The coefficients α_{d2} and I_2 vary. The best results are presented according to curve 7 of Figure 6	40.5	47.6	0.52	0.42
		31.0		0.33	

Note: Each second line of the stage presents the number of estimates of N_{em} and q_m that are simultaneously within the measurement precision.

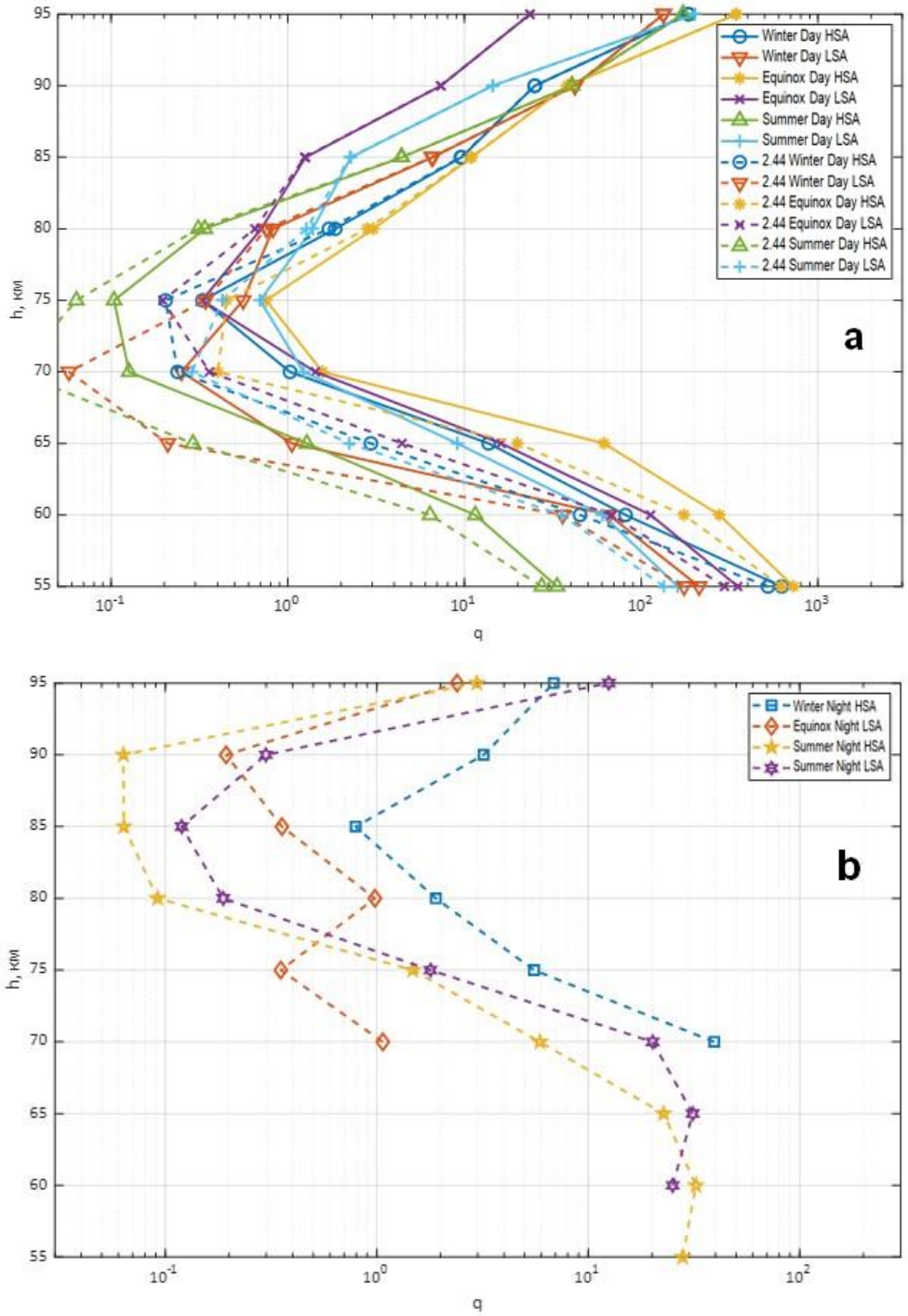

Figure 9. Variations in daytime $q(h)$ under various heliogeophysical conditions for two values I_1=0.33 s^{-1} (solid curves), I_1=2.44 s^{-1} (dashed curves) (*a*); variations in nighttime $q(h)$ under various heliogeophysical conditions $I_1=I_2=0$ (*b*)

CONCLUSION

The calibration of the semi-empirical method based on two sets of experimental data, the analogue of which, even approximate, we have not found in the scientific literature, has shown that it can be reliably applied to a wide range of heliogeophysical conditions in undisturbed and disturbed D-region. To reach a better agreement between the model calculations and the experiment, it is necessary to use current concepts of the temperature T dependent rates and the rates of photodetachment from O_2^-, determined by χ and h. The unknown α_{d2} and I_2 can be considered as freely variable parameters, of course within due limits. The calculations of Δq and ΔN_e are noticeably affected by $T(h)$. Thus, this distribution should be carefully chosen, taking into account latitude, season, time of day, solar and magnetic activity.

In the quiet ionosphere, nighttime $q(h)$, calculated from experimental mean $<N_e>$, differ significantly from daytime values, especially in the shape of curves in summer and at the equinox. This once again confirms the well-known opinion about the unresolved problem of D-region ionization sources under such conditions.

Experimental data obtained during SPE on November 2–5, 1969 and HANE shows a decrease in N_{eexp} at all h for $q_{exp} \approx (1.3–2)\cdot 10^2$ cm^{-3} s^{-1}, followed by their increase with increasing q. This behavior of N_e is mainly confirmed by calculations with the semi-empirical method, but for a wider range of q variations. Further analysis is required for a theoretical understanding of the detected effect and a better agreement between the model estimates and the experiment.

The use of new values of I_1 for daytime launches 1–6 shifts curves $\Delta N_e(h)$ to the left and Δq to the right, which improves the theoretical estimates and shifts them to the region of instrumental precision for N_{eexp} and q_{exp} measurements.

To compare the calculations with the experiment, two methods are employed — point and geometric. The results are somewhat contradictory: in some cases, the best agreement is obtained by the former method; in others, by the latter. It is, therefore, reasonable to adopt both methods, although in general the geometric one is preferable.

When estimating unknown α_{d2} and I_2, it is best to use experimental data on $\alpha_{exp}(h)$, calculated from Equation (14). Various calculations (see Figure 5) show that it is necessary to change both parameters simultaneously according to h. We have demonstrated that a reasonable choice of $\alpha_{d2}(h)$ and $I_2(h)$ provides a good agreement of calculations with experiment. The selected values of these parameters are interpreted from the aeronomic point of view.

In general, the studies carried out here suggest that the semi-empirical method can be widely adopted. In some cases, the final results will be only qualitative; in many others, fairly satisfactory quantitative estimates. In the future, it is planned to use the calibrated method for calculating propagation of superlong and long radio waves.

We thank S.Z. Bekker for some calculations and discussion of the results, A.N. Lyakhov for attention and interest in the work, as well as V.V. Yakim for assistance in preparing the manuscript for publication.

The work was carried out under government assignment FMWN-2022-0021.

REFERENCES

Avdyushin S.I., Alpatov V.V., Vetchinkin N.V., Romanovskij Yu.A. Active experiments and anthropogenic effects in near-Earth space: Methodology, equipment, results. *Space Model*. 2007, vol. 2, pp. 891–917. Moscow, 2007. (In Russian).

Bekker S.Z. Probabilistic-statistical model of low undisturbed mid-latitude ionosphere verified according to data of ground-based radio physical measurements. *Thesis Abstract*. Moscow, IDG RAN Publ., 2018, 26 p. (In Russian).

Bekker S.Z., Ryakhovsky I.A., Korsunskaya J.A. Modeling of the lower ionosphere during solar X-ray flares of different classes. *J. Geophys. Res.: Space Phys*. 2021, vol. 126, no. 2, e2020JA028767. DOI: 10.1029/2020JA028767.

Boyarchuk A.K, Karelin A.V., Shirokov R.V. *Basis Model of the Ionized Atmosphere Kinetics*. Moscow, 2006, 203 p. (In Russian).

Danilov A.D., Rodevich A.YU., Smirnova N.V. Parametric model of the D-region, taking meteorological effects into account. *Geomagnetizm i aeronomiya* [Geomagnetism and Aeronomy]. 1991, vol. 31, no. 5, pp. 881–885. (In Russian).

Danilov A.D., Rodevich A.YU., Smirnova N.V. Problems with incorporating a new D-region model into the IRI. *Adv. Space Res*. 1995, vol. 15, no. 2, pp. 165–167.

Friedrich M., Torkar K.M. FIRI: A semiempirical model of the lower ionosphere. *J. Geophys. Res*. 2001, vol. 106, no. A10, pp. 21409–21418.

Friedrich M., Pock C., Torkar K. FIRI-2018, an updated empirical model of the lower ionosphere. *J. Geophys. Res.: Space Phys*. 2018, vol. 123, pp. 6737–6751. DOI: 10.1029/2018JA025437.

Gordillo Vazquez F.J. Air plasma kinetics under the influence of sprites. *J. Phys. D: Applied Phys*. 2008, vol. 41, p. 234016.

Haerendel G., Sagdeev R.Z. Artificial plasma jet in ionosphere. *Adv. Space Res*. 1981, vol. 1, no. 2, p. 29–44. DOI: 10.1016/0273-1177(81)90270-2.

Ivanov-Kholodny G.S., Mikhailov A.V. Prediction of the State of the Ionosphere (Deterministic Approach). Leningrad, Hydrometeoizdat Publ. 1980, 190 p. (In Russian).

Kozlov S.I. Ion kinetics in the ionosphere night-side D-region. *Kosmicheskie issledovaniya* [Cosmic Res.]. 1971, vol. 9, no. 1, pp. 81–90. (In Russian).

Kozlov S.I. *Aeronomy of Artificially Disturbed Earth's Atmosphere and Ionosphere*. Moscow, TORUS-PRESS, 2021. 268 p. (In Russian).

Kozlov S.I., Smirnova N.V. Methods and means of creating artificial formations in the circumterrestrial medium and estimation of the characteristics of arising perturbations. I. Methods and means of creating artificial formations. *Kosmicheskie issledovaniya* [Cosmic Res.]. 1992a, vol. 30, no. 4, pp. 495–523. (In Russian).

Kozlov S.I., Smirnova N.V. Methods and means of creating artificial formations in the circumterrestrial medium and estimation of the characteristics of arising perturbations. II. Estimation of the characteristics of artificial perturbations. *Kosmicheskie issledovaniya* [Cosmic Res.]. 1992b, vol. 30, no. 5, pp. 629–693.

Kozlov S.I., Lyahov A.N. Photodetachment rates for O^- and O_2^- in the D layer of the ionosphere as function of solar zenith angle and solar activity. *Solar-Terr. Phys.* 2023, vol. 9, iss. 4, pp. 95–98. DOI: 10.12737/stp-94202312.

Kozlov S.I., Lyahov A.N., Bekker S.Z. Key principles of constructing probabilistic statistical ionosphere models for the radiowave propagation problems. *Geomagnetism and Aeronomy*. 2014, vol. 54, iss. 6, pp. 750–762.

Kozlov S.I., Bekker S.Z., Lyahov A.N., Nikolaishvili S.S. A semiempirical approximate method for investigating some problems of the aeronomy of the D-region of the ionosphere. I. Basic Principles of Method Development and Basic Equations. *Geomagnetism and Aeronomy*. 2022, vol. 62, iss. 5, pp. 607–613. DOI: 10.1134/S0016793222050073.

Nesterova I.I., Ginzburg E.I. *Catalogue of electron density profiles of the ionosphere D region*. Novosibirsk, 1985, 210 p. (In Russian).

Proc. COSPAR Symposium on Solar Particle Event of November 1969. AFCRL. 72. 0474. Special report N144. Ed. J.C. Ulwick. 1972, 703 p.

Sellers B., Stroscio M.A. Rocket-measured effective recombination coefficients in the disturbed D-region. *J. Geophys. Res*. 1975, vol. 80, no. 16, pp. 2241–2246.

Smirnova N.V., Kozlov S.I., Vlaskov V.A. Special-purpose aeronomic model for investigating the artificial modification of the middle atmosphere and lower ionosphere. II -

Comparison of calculation results with experimental data. *Kosmicheskie issledovaniya* [Cosmic Res.]. 1990, vol. 28, no. 1, pp. 77–84. (In Russian).

Swider W. Aeronomic aspects of the polar D-region. *Space Sci. Rev.* 1977, vol. 20, pp. 69–114. DOI: 10.1007/BF02186894.

Swider W., Dean W.A. Effective electron loss coefficient of the disturbed daytime D-region. *J. Geophys. Res.* 1975, vol. 80, iss. 13, pp. 1815–1819. DOI: 10.1029/JA080i013p01815.

Swider W., Narcisi R.S., Keneshea T.J., Ulwick J.C. Electron loss during a nighttime PCA event. *J. Geophys. Res*. 1971, vol. 79, iss. 19, pp. 4691–4694.

Swider W., Keneshea T.J., Foley C.I. An SPE-disturbed D-region model. *Planetary and Space Sci*. 1978, vol. 26, iss. 9, pp. 883–892. DOI: 10.1016/0032-0633(78)90111-3.

Van Gaens W., Bogaerts A. Kinetic modelling for an atmospheric pressure argon plasma jet in humid air. *J. Phys. D: Appl. Phys*. 2013. v. 46, no. 27, p. 275201. DOI: 10.1088/0022-3727/46/27/275201.

Whitten R.C., Poppoff I.G., Edmonds R.S., Berning W.W. Effective recombination coefficients in the lower ionosphere. *J. Geophys. Res*. 1965, vol. 70, iss. 7, pp. 1737–1742. DOI: 10.1029/JZ070i007p01737.

World Meteorological Organization (WMO). Global Ozone Research and Monitoring Project Report. 1985, no. 16, 392 p.

Original Russian version: Kozlov S.I., Nikolaishvili S.Sh., published in Solnechno-zemnaya fizika. 2024. Vol. 10. No. 4. P. 79–90. DOI: 10.12737/szf-104202409.

How to cite this article

Kozlov S.I., Nikolaishvili S.Sh. Semi-empirical method of studying the D-layer aeronomy. II. Evidence-based calibration of the method. *Solar-Terrestrial Physics*. 2024. Vol. 10. Iss. 4. P. 72–83. DOI: 10.12737/stp-104202409.